Exfoliation and dispersion of 2D materials in polar solvents: A molecular simulation approach

Titas Kumar Mukhopadhyay and Ayan Datta*

School of Chemical Sciences, Indian Association for the Cultivation of Science, Jadavpur, Kolkata-700 032, India

E-mail: spad@iacs.res.in

Among the various novel synthetic routes for 2D materials, liquid phase exfoliation (LPE) has emerged to be most effective. Nevertheless, the key material properties guiding the hierarchical steps for LPE are still unknown. Herein, through all atom molecular dynamics simulations and free energy calculations we compare the exfoliation and re-aggregation tendencies of five common 2D materials namely graphene, blue and black phosphorene, hexagonal boron nitride and molybdenum disulfide, in polar solvents water and DMSO. It is revealed that, larger molecules such as DMSO efficiently intercalates between material layers during sonication and interact predominantly through van der Waals interactions, thereby stabilizing the dispersed state and increasing the exfoliation efficacy. Small molecules e.g. water cannot stabilize the individual 2D layers through solvation and therefore, the intercalated water molecules are easily ejected from in between the nanosheets, eventually leading to re-combination. Solvation free energy calculations show that solvation of a single nanosheet is thermodynamically favorable in both solvents although the nature of balance between the enthalpic and entropic parts is fundamentally different for water and DMSO. From the calculation of exfoliation free energies it is shown that the ease of exfoliation follows the trend: MoS_2 > Blue Phosphorene > Black Phosphorene > Hexagonal Boron Nitride > Graphene.

Keywords: 2D Materials, liquid phase exfoliation, molecular dynamics, potential of mean force, solvation free energy.

Introduction

Since the discovery of graphene, tremendous research efforts have been endeavored towards the synthesis and development of 2D materials because of their outstanding physico-chemical properties along with substantially large surface area which make them suitable candidates for a variety of applications including nano-device fabrication[1–5]. Till date, a plethora of avenues have been explored in connection with the synthesis of 2D nanomaterials, chemical vapor deposition (CVD), mechanical exfoliation (ME) and liquid phase exfoliation (LPE) being profoundly important among them[4]. Particularly, ultrasonication assisted liquid phase exfoliation is considerably better compared to the other alternatives, since it does not suffer from low yield and can be performed at room temperature[6–9]. Therefore, a lot of stress has been given to disentangle the necessary qualities of solvent molecules which favor exfoliation of various 2D monatomic layers from their 3D counterparts and hinder the re-aggregation of exfoliated nano-sheets. Searching for good solvents, experimentalists have performed extensive solvent screening for the exfoliation of a large number of 2D materials[9]. In addition, it has been shown by Hernandez and co-workers that, Hildebrand and Hansen solubility parameters in conjunction with surface tension can provide an empirical correlation with the ability of exfoliation[10]. Coleman *et al*. suggested that solvents having surface tensions nearly equal to the 2D materials are able to stabilize their colloidal dispersion after sonication assisted exfoliation[11,12]. However, these parameters are phenomenological and cannot shed light into the molecular details of the interactions between solvent molecules and the atomically thin layers of 2D materials.

Molecular dynamics simulation is a better alternative in this aspect, since it can identify the molecular scale interactions quite precisely and estimate the energetics involved in hierarchical steps of exfoliation. Previously, MD simulations have successfully been applied to identify the exfoliation tendencies and free energies of nonpolar 2D materials graphene, black phosphorene and molybdenum disulfide[13–18]. In a recent study we investigated the role of solvent molecules in the LPE of polar 2D material hexagonal boron nitride and

elucidated the essential characteristics of solvent molecules responsible for exfoliation as well as re-aggregation[19]. However, benchmarking the 2D materials with respect to their exfoliation tendencies in a given solvent is crucial since it can, in principle, provide important aspects of material properties involved in exfoliation, which has not been stressed in previous reports. To this regard, we perform large scale classical molecular dynamics simulations to compare some of the state-of-the-art materials according to their exfoliation efficiencies toward two common polar solvents, namely, dimethyl sulfoxide (DMSO) and water. DMSO has previously been identified as "good" solvent for the exfoliation of a variety of 2D materials including graphene, h-BN and phosphorene while water is experimentally been found to behave "poorly"[6,7,15,16]. Graphene and blue as well as black phosphorene are taken as nonpolar materials while 2D materials h-BN and molybdenum disulfide (MoS_2) are considered as polar materials for the present purpose. A large set of solvent diffusion and exfoliation simulations have been performed to identify the interactions between 2D materials and solvent molecules with different sizes. Estimation of the solvation free energies for single nanosheets in the solvents gives profound idea regarding the stabilities of the dispersed states. Further, calculation of the free energies for exfoliation in gas phase and in solvated states helps to identify the solvent preference. DMSO is shown to be more effective as an exfoliating solvent due to the strong dispersion interactions of 2D materials with the sulfur atoms for nonpolar materials while for polar nanosheets, dispersion interactions are accompanied by long range electrostatic interactions, although the effect of the latter is minor. Nevertheless, size of the solvent molecules is found to play an important role during exfoliation, larger solvent molecules producing stable and less interacting dispersed states. We believe, the present article provides deep insights into the specific nature and thermodynamics of interactions between the materials and solvent molecules responsible for increasing the shelf-life of the dispersed state of 2D materials.

2. Computational details

We perform three different kinds of simulations namely simulation of solvent diffusion and exfoliation, potential of mean force for exfoliation and solvation free energy calculations. In order to compare the interactions and the free energies for exfoliation of different 2D materials in water and DMSO, rectangular bilayers of graphene, h-BN, black Pn, blue Pn and MoS_2 considered, each consisting of similar number of interaction sites.

2.1. Simulation of solvent diffusion and exfoliation

For solvent diffusion simulations, each of the bilayers are placed at the center of simulation boxes of dimension 6×8×6 nm^3 along the XY plane where the long axes of the nanosheets are oriented along the Y axis. The sheets are then vertically separated by 6 Å and 10 Å distances respectively and solvated with water. However, for DMSO, only 10 Å separated bilayers are taken. Periodic boundary conditions are applied in all three directions and sizes of the boxes are such that the interactions with their periodic images can easily be avoided. We performed energy minimization for 20000 steps using the conjugate gradient method and after that, each system is equilibrated for 10 ns in the canonical (NVT) ensemble at 300 K so that solvent molecules can diffuse and intercalate between the sheets. Following this, a 20 ns production simulation is performed for each system using the isothermal-isobaric (NPT) ensemble at 300 K and 1 atmospheric pressure. During all these simulations, each atom of both the sheets is harmonically constrained with a force constant of 10 kcal/mol/Å^2. To model exfoliation, the last frame of the diffusion simulation is taken in each case, harmonic constraints are removed from the upper layer and production simulations are performed for 80 ns at 300 K using NPT ensemble.

In all the simulations, isothermal conditions are maintained engaging Langevin dynamics with a damping coefficient of 5 ps^{-1} [20]. Langevin piston method is employed to maintain a constant pressure of 1 atm. For this purpose, a 100 fs piston period, 50 fs damping time constant and 300 K piston temperature is considered[21]. Particle mesh Ewald (PME) method with 1 Å grid is used to calculate the periodic electrostatic interactions[22]. A 2 fs time step was used to integrate classical equations of motions using the Velocity Verlet algorithm[23]. The SHAKE algorithm is employed to hold rigid covalent bonds involving hydrogen atoms. Non-bonded interactions

are calculated having a cutoff distance of 12 Å. The atomic coordinates are stored after every 10 ps for the trajectory analyses. Graphene and h-BN nanosheets are built with the VMD nanotube builder plug-in and the other 2D nano-sheets are obtained by periodically propagating their respective experimental unit cells[24]. To eliminate dangling bonds, valencies of the terminal atoms are fulfilled by adding hydrogen atoms. Packmol utility is used for the preparation of all initial configurations, NAMD 2.10 for all classical molecular dynamics simulations, VMD for visualization and our in house Tcl scripts as well as VMD plug-ins for the analysis of data[24–26]. We use TIP3P model for water and CHARMM General Force Field (CGenFF) parameters for DMSO[27,28]. Force field parameters for the 2D materials except blue phosphorene are taken from our previous works and recent literatures[15,16,19,29,30]. For blue phosphorene, the crystal bond length, angle and dihedrals are maintained and the same Lennard-Jones parameters as black phosphorene are used.

2.2. Calculation of potential of mean force (PMF)

The reversible free energy changes for exfoliation are calculated in terms of potential of mean forces (PMF), using the adaptive biasing force (ABF) method implemented in NAMD[31]. For the calculation of exfoliation PMF's through peeling mechanism, vertical distances (d_z) between the centre of masses of the two nano-sheets are chosen as the reaction coordinates which are divided into several overlapping windows, each having width of 0.1 nm. Each of these windows is further divided into small bins of 0.02 nm width and a biasing force is applied. A harmonic force of 500 kcal/mol/Å is applied to the upper and lower boundaries of the reaction coordinates in all the windows so that the concerned atoms cannot go beyond these boundaries. Finally, a 3 ns production ABF simulation is performed for each window at 300 K using NPT ensemble. During PMF calculations, each atom of bottom layer is harmonically constrained with a force constant of 10 kcal/mol/$Å^2$ while the top layer is free.

2.3. Calculation of solvation free energies

The alchemical transformation module in conjunction with the free energy perturbation method (FEP), as implemented in NAMD 2.12 is used for the calculation of the solvation free energies of different nano-sheets[32]. First, single nanosheets are solvated in water and DMSO boxes of dimensions 6×8×4 nm^3 and equilibrated at 300 K using NPT ensemble for 10 ns. Then, with the last frame of these simulations, two different transformations are carried out for each system namely coupling of the nanosheets with solvent (forward transformation) and the decoupling of the nanosheets from a solvated state (reverse transformation). Each of the coupling and decoupling simulations are performed using 20 intermediate states corresponding to the uniform variation of the coupling parameter (λ) between 0 and 1 ($\Delta\lambda$ = 0.05). The total free energy for the transformation is a continuous function of λ and is calculated as an ensemble average over configurations representative of the initial state

$$\Delta G_{solvation} = -k_B T \sum_{k=1}^{N} \ln \left\langle \exp\left[-\frac{H(r,p;\lambda_{k+1}) - H(r,p;\lambda_k)}{k_B T} \right] \right\rangle_k$$

where $H(r, p; \lambda_k)$ is the Hamiltonian of the state corresponding to λ_k, $\langle \cdots \rangle$ represents ensemble average and N stands for the number of intermediate state between the gaseous and solvated states. The soft-core van der Waals radius shifting coefficient is set to 6 $Å^2$ to avoid 'end point catastrophes' when λ is close to 0 or 1[33,34]. To obtain better performance, electrostatic and Lennard-Jones potentials are decoupled separately. For each intermediate state, equilibration is performed for 200 ps and ensemble average is calculated for another 2 ns. Bennett Acceptance Ratio (BAR) method is adopted for error analysis of free energy data for different λ domains[35].

3. Results and discussion

3.1. Exfoliation of 2D materials

In experiments, a layered material is sonicated in a solvent so that the stacked layers undergo vertical expansion under the influence of external force, thereby leading to solvent infiltration between the layers which in turn facilitate exfoliation. To computationally mimic the situation, we adopted a two-step simulation protocol namely solvent diffusion and solvent induced exfoliation simulations. In the diffusion simulations, we take vertically expanded bilayers of different layered materials and simulations are performed in

DMSO and water. Two different vertical separations are considered (6 Å and 10 Å) in water while for DMSO only 10 Å expanded bilayers are taken for each material. We apply a weak harmonic constraint to both the layers so that small displacements due to structural organization are allowed but complete re-aggregation is prevented. During the 10 ns of NVT and another 10 ns of NPT simulations, solvent molecules infiltrate the space between the nano-sheets and the density becomes equilibrated. The last frames of these simulations are used for the 80 ns exfoliation simulations during which the constraint over the upper layer is removed. For a better comparison, we first discuss the results obtained in DMSO and then we show how the nano-sheets aggregate in water.
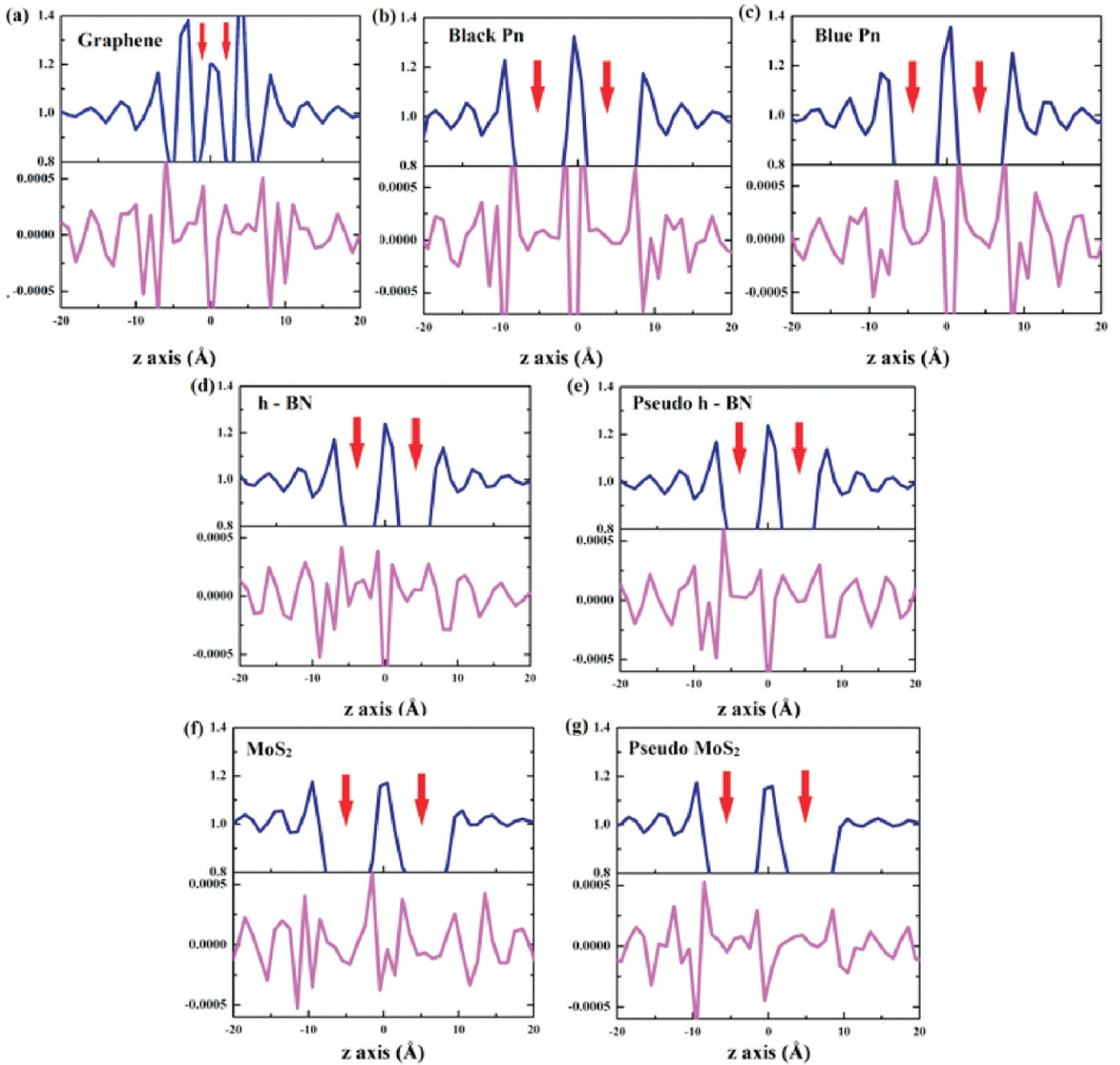
Fig. 1(a-g) shows the average number density profiles relative to the bulk (ρ/ρ_0, dark blue lines) and the average charge density profiles (pink lines) of the DMSO molecules along z-axis for different nano-sheet bilayers during the last 20 ns of the exfoliation simulations. It is observed that a single layer of solvent molecules are adsorbed on each side of the surfaces giving rise to a monolayer of confined DMSO molecules ($z \approx 0$) between each of the bilayers, indicated by large density peaks. The amplitudes of the number density oscillations of the intercalated DMSO molecules within the first solvation sphere are much higher and sharper for graphene, black and blue phosphorene ($\rho/\rho_0 > 1.3$, see Fig. 1(a-c), blue lines) compared to those for h-BN, MoS_2 and their nonpolar analogs ($\rho/\rho_0 < 1.2$, see Fig. 1(d-g), blue lines). It can be related to the weaker interaction of these monotypic nonpolar surfaces with the solvent molecules which cannot disrupt the intermolecular interaction between the intercalated molecules. On the other hand, polar h-BN and especially MoS_2 easily perturbs the solvent-solvent interactions to make density amplitudes lower. In addition, the charge density profiles shed light into the molecular ordering near the immediate vicinity of the layers. As observed in Fig. 1(a-g), the solvent layers adjacent to each of the surfaces have a high positive charge density. According to the CHARMM force field the sulfur atom and each of the methyl groups in DMSO bear a positive charge of +0.31e and +0.12e respectively and therefore, it is clear that the polarizable sulfur atoms and the methyl groups have a higher affinity of interaction towards the surfaces. The charge density fluctuation gradually attenuates as we move towards the bulk, demonstrating the progressive loss of the solvation structure. It is noteworthy that, similar to number density profiles, the charge density fluctuations are much higher in amplitude near graphene, black and blue phosphorene surfaces compared to h-BN and MoS_2, which again suggests a higher degree of perturbation towards the solvent ordering inflicted by the later surfaces which operate through the loss of intermolecular interactions among DMSO molecules. Moreover, due to partial positive charges over B and Mo centers in h-BN and MoS_2 respectively, positive sulfur is repelled so that it cannot strongly accumulate on the surface, leading to the depletion of charge ordering. Indeed, the radial distribution functions depicted in Fig. 2(a-c) shows that the probability of occurrences of sulfur and carbon is higher than oxygen near typically nonpolar surfaces such as graphene and black Pn, indicated by the closer solvation peaks of the former atoms, while for polar MoS_2, the characteristic distribution peak for oxygen appears first followed by carbon. In fact, sulfur has no well-defined peak near MoS_2 surface, which is a prominent indication of the feeble adsorption of sulfur atoms of DMSO.

During exfoliation simulations, the free nano-sheet undergoes thermal and solvent induced fluctuations along all possible directions. However, we observe neither the recombination of the layers through expulsion of intercalated solvents nor the complete exfoliation of the upper layer in any of our simulations in DMSO. The exfoliation tendencies of the free nano-sheets can qualitatively be compared through their self-diffusion coefficients (D^{exfol}) for the entire duration of the production simulations, which are represented by Table 1. The D^{exfol} values show the order MoS_2 > pseudo MoS_2 > h-BN > pseudo h-BN $\approx$ graphene > blue Pn > black Pn which are similar in order to those calculated in previous literatures and can be considered as a first approximation towards the ranking in their exfoliation abilities[16,19].

To assess the dynamical nature of the intercalated DMSO molecules, we calculated the diffusion coefficients of the bulk and intercalated solvent molecules and Table 2 represents the same. Table 2 clearly shows that the diffusion coefficients of the intercalated molecules are significantly reduced (0.13–

Fig. 1. Average number density relative to the bulk (dark blue lines) and average charge density (pink lines) of the DMSO molecules along z-axis for (a) graphene, (b) black Pn, (c) blue pn, (d) h-BN, (e) pseudo h-BN, (f) MoS_2 and (g) pseudo MoS_2 respectively. $z = 0$ represent the center of the simulation boxes and the positions of the layers are indicated by bold red arrows in each figure. Note that, relative number densities are unit less and the charge densities are of the order 10^{-5} e/Å^3.

0.33×10^{-5} cm^2 s^{-1}) compared to bulk (0.79×10^{-5} cm^2 s^{-1}) and therefore, these molecules, being more dynamically constrained, behave significantly different from the bulk. Recently, Nie *et al.* showed that a monolayer of water molecules confined within black Pn sheets can undergo melting-freezing transitions depending on the relative orientation of the sheets[36]. Our results are also in line with their conclusions. Moreover, apart from the loss of a degree of freedom along the direction perpendicular to the sheets, the monolayer of intercalated molecules become more confined due to the
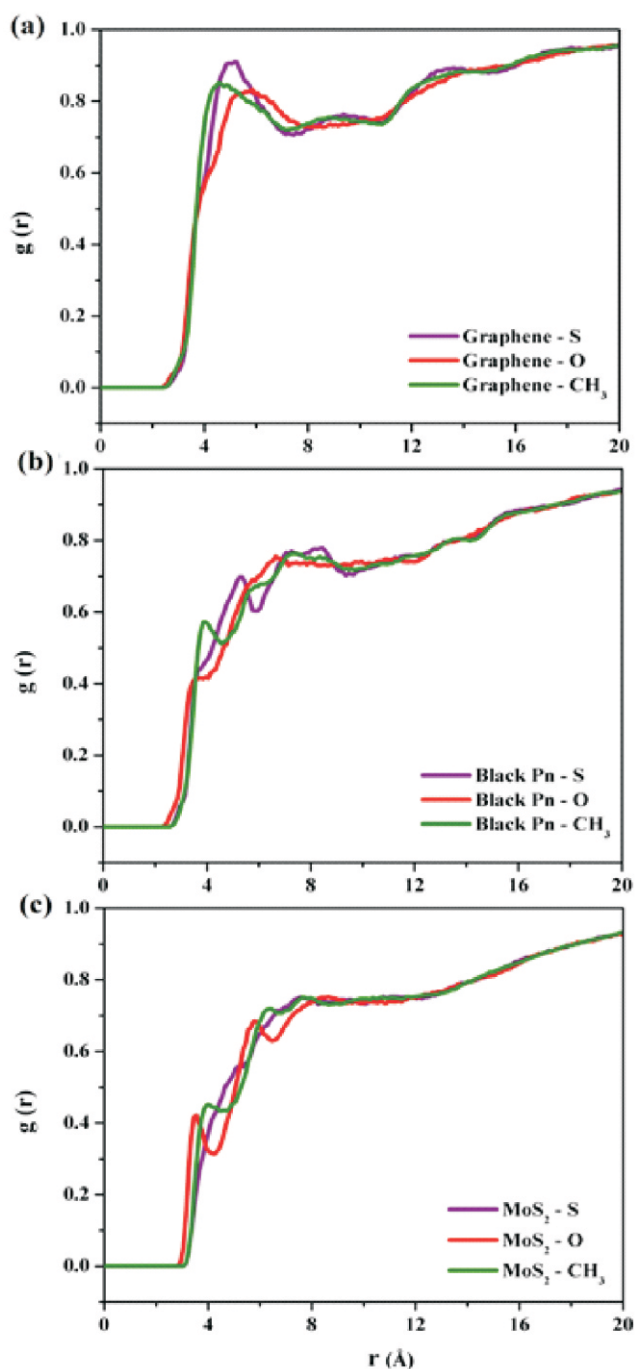
Fig. 2. Radial distribution functions between (a) graphene, (b) black Pn and (c) MoS$_2$ surfaces and the interacting groups of DMSO. The probability of occurrence of positively charged sulfur atom and methyl groups is higher than oxygen near nonpolar graphene and black Pn surfaces, indicated by sharp peaks. On the contrary, for polar MoS$_2$, the radial distribution peak of oxygen is closest to the surface, indicating feeble adsorption of methyl groups and sulfur atoms on the surface.

Table 1. Self diffusion coefficients of different exfoliating (unconstrained) nano-sheets in DMSO

Nanosheet	D^{exfol} (×10^{-13} cm^2 s^{-1})
MoS$_2$	40.3
Pseudo MoS$_2$	34.1
h-BN	30.0
Pseudo h-BN	20.5
Graphene	20.2
Blue Pn	9.3
Black Pn	6.1

Table 2. Diffusion coefficients of the DMSO molecules intercalated between the different bilayers of 2D materials during the exfoliation simulations

| Nanosheet	$D^{intercal}$ (×10^{-5} cm^2 s^{-1})
MoS$_2$	0.26
Pseudo MoS$_2$	0.23
h-BN	0.33
Pseudo h-BN	0.18
Graphene	0.22
Blue Pn	0.17
Black Pn	0.13
Bulk (average)	0.79
Bulk (experimental)	0.61

steric compression of the nano-sheets when interlayer binding is high, as indicated in previous literatures. In contrast, if the solvent molecules are efficient to screen the interlayer interactions, they move relatively freely between the sheets. The values of $D^{intercal}$ for DMSO molecules entrapped between polar MoS$_2$ and h-BN sheets are higher compared to those observed for the nonpolar materials graphene and phosphorene. In fact, the same trend, as observed for the self-diffusion coefficients, is nearly conserved for the $D^{intercal}$ values. Pseudo h-BN and pseudo MoS$_2$, being non-polar, have smaller self-diffusion coefficients compared to their charged analogs and the solvent molecules confined in between them are also less dynamic. Therefore, their behaviors approach that of other monotypic 2D crystals.

Although the density profiles and the diffusion coefficients give a preliminary estimate of the propensities of the nanosheets to exfoliate, but elucidation of the energetics involved in the systems give more appreciable insights. Fig. 3(a) shows the interlayer interaction energies scaled to the

surface area for different materials in DMSO during the exfoliation simulations and they follow the order MoS_2 > pseudo MoS_2 ≈ pseudo h-Bn ≈ blue Pn > black Pn > graphene > h-BN >. However, the scaled nanosheet-solvent interaction energies follow a different trend: MoS_2 > h-BN > pseudo MoS_2 > pseudo h-Bn > blue Pn > black Pn > graphene, as shown in Fig. 3(b). Clearly, these two trends are not commensurate to each other. Under solvent intercalated situation, blue and black phosphorenes have better interlayer binding as well as better interaction with the solvent molecules compared to graphene through better dispersion interactions ($\in_p$ > $\in_c$). However, the slightly lower interaction energies of black Pn compared to blue Pn can be attributed to the greater undulation in the former surface which makes the phosphorus atoms more impenetrable to interact with solvent molecules. This result is also supported by previous DFT calculations showing higher binding energies of small molecules over blue Pn surface[37,38]. The charged nanosheets h-BN and MoS_2, interact more with the solvents compared to the uncharged materials, having a large contribution from long ranged electrostatics. Nevertheless, the significantly high interaction energies of pseudo h-BN and MoS_2 with DMSO suggest that the solute-solvent interactions for these nano-sheets are predominantly (~70%) van der Waals type, electrostatic inter-

actions are just a favorable addition (~30%). On the other hand, the nature of the interlayer interactions for these two polar materials opposes each other. MoS_2 has the highest interlayer interaction energy among all the materials but for h-BN the interaction energy is positive. We identified this behavior of h-BN in a recent article which was attributed to the solvent induced motion of the weakly bound sheets[19]. However, MoS_2, being larger in size and having greater inter-sheet dispersion compared to BN, induces greater attraction between the sheets when separated by a layer of DMSO molecules. Also, Fig. 3(b) shows that, the intercalated molecules have a significantly large share towards the total nanosheets solvent interaction energies. Therefore, it is obvious that, the dynamically restricted molecules residing between the sheets provide a barrier towards the recombination of the nano-sheets, provided that the van der Waals interaction between the sheets and the confined solvent layer is significantly high.

Water, on the other hand, shows strikingly different results compared to DMSO. For the first 10 nanoseconds of NPT equilibration wherein both of the layers are constrained, all of the 6 Å and 10 Å separated sheets are intercalated by a monolayer and bilayer of water molecules respectively except black Pn, which maintained a monolayer of water in both of the simulations. However, as soon as the exfoliation
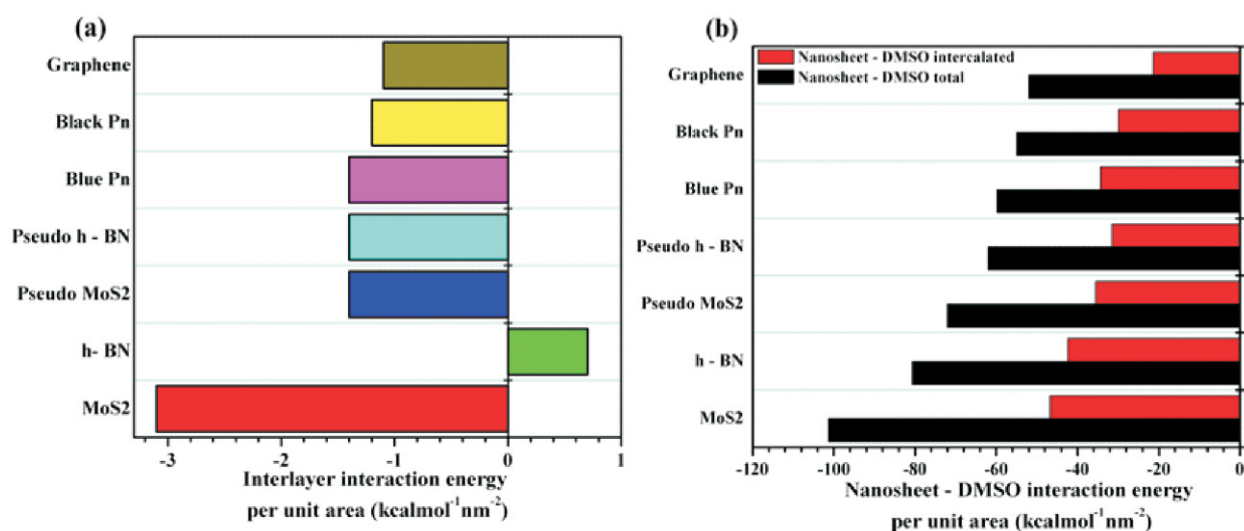

Fig. 3. (a) Interlayer interaction energies between the two nano-sheets and (b) nanosheet DMSO total interaction energy and the contribution from the interaction energies with intercalated molecules. For a better comparison, all the interaction energies are scaled to the surface area.

simulations started, some of the bilayers began to collapse through the expulsion of intercalated water molecules except h-BN and pseudo h-BN and Fig. 4(a-c) shows typical snapshots from the consecutive steps for the collapse of an initially 10 Å separated bilayer graphene. Fig. 5(a) and 5(b) shows the time evolution of the vertical distances between the initially 6 Å and 10 Å separated bilayers respectively during the first 60 ns of the exfoliation simulations. It is seen that, graphene sheets expel all the intercalated water and collapse extremely fast within only 20 ps and 800 ps respectively for 6 Å and 10 Å separated cases, indicating a high inclination towards re-aggregation. The other sheets separated by a monolayer of water (6 Å separation), also recombine but at different timescales, except h-BN, as shown in Fig. 5(a). For 10 Å separated bilayers, none of them combine completely other than graphene, maintaining a stable monolayer (MoS_2) or bilayer (all others) of water molecules which is clearly due to an interplay among the reduced

interlayer attractions between the solvent intercalated nano-sheets as well as due to the enhancement of nanosheet-intercalated solvent interactions. Therefore, we show that, water acts as a bad solvent compared to DMSO in the liquid phase exfoliation experiments for all the 2D material considered in this study, as the solvent intercalated nano-sheets produced through sonication would have a spontaneous tendency to reaggregate in water unlike DMSO. Additionally, the time scale of aggregation is clearly dependent on the vertical separation between the solvent intercalated sheets as well as the number of layers of solvent molecules entrapped between and therefore, we speculate that the other nano-sheets would recombine in water if simulations are continued for extended timescales. This is evident from the simulation with black Pn, which, despite of being intercalated by a monolayer of water in both 6 Å and 10 Å separations, only recombine in the former simulation but not in the latter one within the 60 ns timescale of our exfoliation simu-
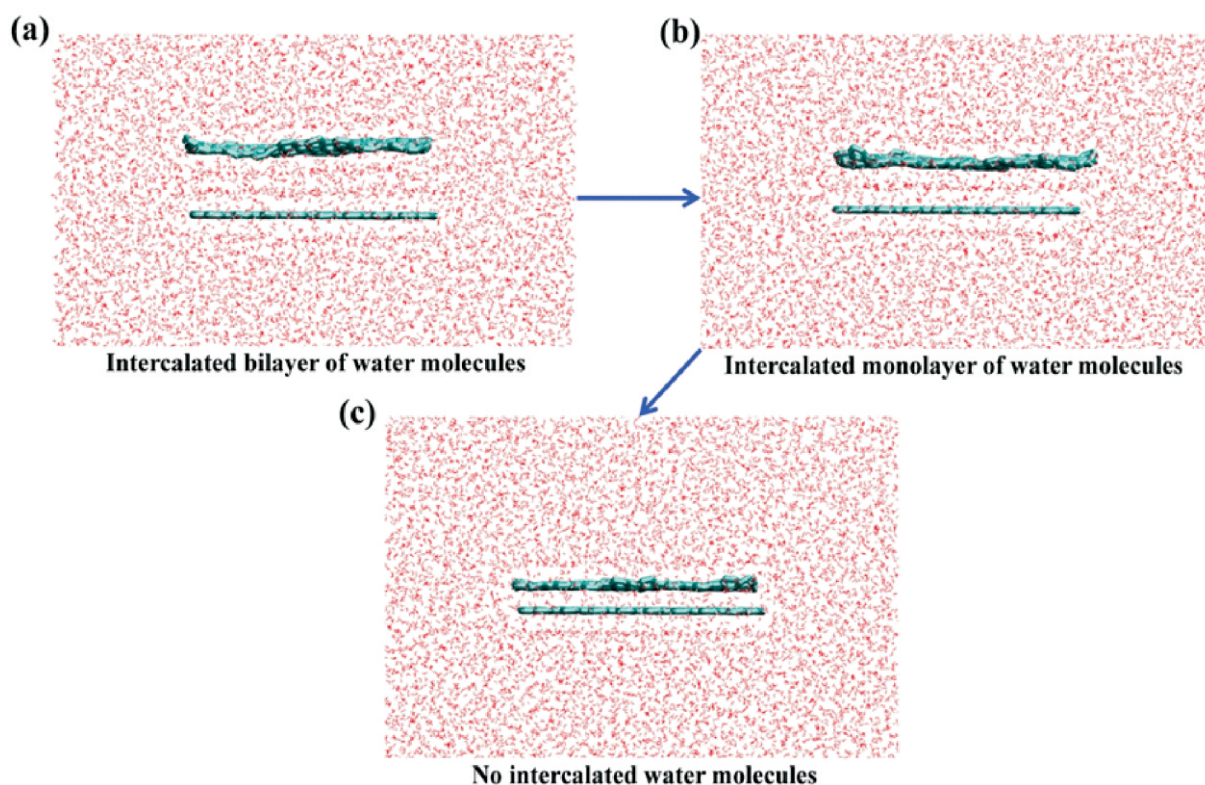
Fig. 4. (a-c) Snapshots for the sequential release of intercalated water molecules from in between graphene layers during exfoliation simulations, leading to the collapse of the nano-sheets into a stacked conformation.
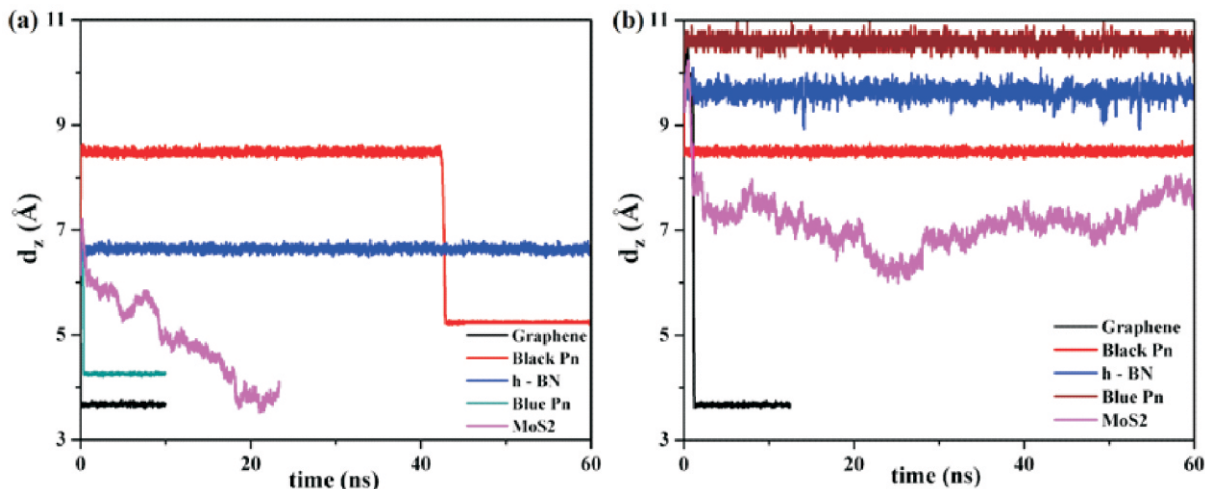
Fig. 5. Time evolution of the vertical distances (d_z) between the different bilayer models during the first 60 ns of the exfoliation simulations in water having initial separation of (a) 6 Å and (b) 10 Å respectively. Note that, we stopped the simulations if complete re-aggregation occurred before 80 ns.

lations. Note that, as the solvent intercalated bilayers undergo aggregation at different timescales and do not show similar behavior, comparison between the dynamical properties of the intercalated molecules is not performed.

3.2. Free energy for solvation

After complete exfoliation, the tendency of the individual monolayers to re-aggregate is certainly dependent on the stability of the exfoliated sheets in the solvent, a higher degree of stabilization indicating a lesser tendency towards recombination. To assess how solvation contribute towards the dispersion of different 2D materials, we calculate the Gibbs free energy changes (ΔG_{sol}) associated with the solvation of per unit area of a single nanosheet (ΔG_{sol}) in water as well as in DMSO (see Fig. 6 and Table 3). It is seen that, ΔG_{sol} is negative for all the solute monolayers in both of the solvents, ensuring the thermodynamic feasibility of the processes. The solvophilicity of the materials can, in principle, be estimated from the magnitude of ΔG_{sol}, a more negative value of the same indicating a more solvophilic surface. From Table 3, the solvophilicity of the materials follow the sequence, graphene < black Pn < blue Pn < pseudo MoS$_2$ < pseudo h-BN < h-BN < MoS$_2$ in water and graphene < black Pn < blue Pn < pseudo h-BN < h-BN < pseudo MoS$_2$ < MoS$_2$ in DMSO. The observed trends are very similar and they closely resemble the trends observed for solute-solvent interaction
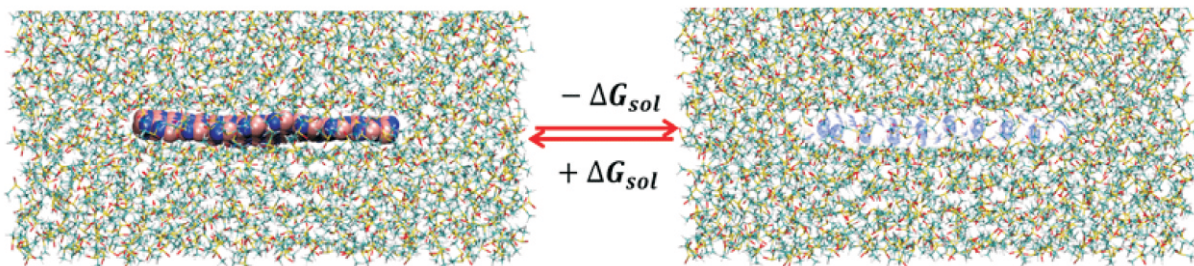
Fig. 6. Schematic alchemical representation of the thermodynamic cycle constructed for the determination of the solvation free energy (ΔG_{sol}) of h-BN in DMSO at 300 K. The (–) and (+) signs indicate decoupling and coupling of the nanosheet from the solvent molecules. The blurred view of the nanosheet on the right hand side indicates a solvent-decoupled state.

Table 3. Change in different thermodynamic potentials accompanying the immersion of per unit area of a single nanosheet into water and DMSO. The potentials are expressed in kcal mol^{-1} nm^{-2}

Solvent	Potential	Graphene	h-BN	Pseudo h-BN	Black Pn	Blue Pn	MoS$_2$	Pseudo MoS$_2$
Water	ΔH_{sol}	1.3	−5.7	−7.4	6.3	17.4	55.7	12.9
	$-T\Delta S_{sol}$	−5.3	−8.8	−3.6	−12.7	−24.5	−86.1	−19.6
	ΔG_{sol}	−4.0	−14.5	−11.0	−6.4	−7.1	−30.4	−6.8
DMSO	ΔH_{sol}	−19.6	−34.8	−46.5	−22.6	−27.9	−36.0	−20.6
	$-T\Delta S_{sol}$	4.7	10.6	22.8	4.6	8.5	−8.3	−19.5
	ΔG_{sol}	−14.9	−24.2	−23.7	−18.0	−19.4	−44.3	−40.1

energies, as mentioned previously (Fig. 2(b)). Decomposition of the solvation free energies into enthalpy and entropy components further demonstrate some unique and distinctly different features of these 2D materials. For all the 2D crystals except h-BN, hydration is forbidden enthalpically, but this penalty is compensated by a largely favorable entropy change, rendering the total Gibbs free energy change negative. Contrarily, for h-BN and pseudo h-BN, hydration is preferred enthapically as well as entropically. In water, the van der Waals interaction between the materials and the solvent is less but some of the intermolecular interactions as well as hydrogen bonding between the water molecules are lost upon interacting with the material surfaces. Therefore, the overall thermodynamic transformation proceeds through an increase in the randomness (entropy) of water molecules, sufficient enough to compensate the enthalpic loss. On the other hand, solvation of the 2D materials in DMSO is enthalpically favored but entropically forbidden (except MoS$_2$). Also, the tendency for solvation for any of the materials is greater in DMSO compared to that in water, as suggested by the more negative values of ΔG_{sol}. DMSO, being sterically bulkier than water and containing a polarizable sulfur site, interacts strongly with the surfaces through dispersion interactions, making solvation enthalpically more favored. Moreover, the DMSO molecules within the vicinity of the surfaces get strongly adsorbed unlike water, thereby reducing the overall conformational freedom of DMSO molecules. As a result, solvation is accompanied with loss of some entropy. It can easily be correlated to the disruption of a well-defined solvation structure due to the polarity of MoS$_2$ surface, as indicated by the number and charge density profiles in Figs. 1(f) and 1(g). Interestingly, h-BN and MoS$_2$ shows more negative ΔG_{sol} in both of the sol-

vents compared to pseudo h-BN and pseudo MoS$_2$ respectively, indicating enhancement in the nanosheet···solvent interactions as a result of partial charges. Notably, the difference in solvation free energies between the polar materials (h-BN and MoS$_2$) and their non-polar analogs (pseudo h-BN and MoS$_2$ respectively) are larger in water compared to that in DMSO. For instance, ΔG_{sol} for MoS$_2$ and pseudo MoS$_2$ are −44.3 and −40.1 kcal mol^{-1} nm^{-2} respectively in DMSO, but −30.4 and −6.8 kcal mol^{-1} nm^{-2} respectively in water. Clearly, when the solvent is DMSO, nano-sheets strongly interact with the molecules through dispersion interactions and electrostatic contribution *en route* to solvation is indeed small. However, in water, van der Walls interactions are overwhelmed by Coulomb interactions and withdrawal of partial charges from the polar nano-sheets result in a larger difference in solvation free energy.

Recently, Chaban *et al.* found that for both graphene and black phosphorene, free energies for solvation in ionic liquids are positive, the small enthalpic gains being largely surpassed by unfavorable entropy changes[39,40]. In contrast to their results, we find that, solvation of 2D nano-sheets in molecular solvents such as water and DMSO proceeds through two thermodynamically opposing mechanisms. For small and weakly interacting solvent such as water, solvation is mostly guided by the entropic factor while in a strongly interacting bulky solvent such as DMSO, enthalpy motivates solvation. Additionally, since the materials maintain qualitatively similar trend for the solvation free energies in both the solvents, therefore, we consider it to be a generalized trend in other solvents unless some particular sites of the solvent preferentially interacts with any material or there is some chemical decomposition of the surface.

3.3. Free energy for exfoliation

Exfoliation of 2D materials is an energy demanding process and to arrange the 2D materials according to their abilities to exfoliate in solvents, we addressed the problem from a thermodynamic standpoint. We calculated the reversible work done to exfoliate a single layer from a bilayer model in both the solvents and also in vacuum, for different 2D materials and these are represented in terms of the potential of mean forces (PMF). We define a quantity $\Delta PMF = \Delta G_{solvent} - \Delta G_{vacuum}$, a positive value of which represents the solvent induced lowering of the free energy barrier for exfoliation[16]. It is worthwhile to mention that, during PMF calculations, choice of the reaction coordinate plays a pivotal role and previous studies have suggested the existence of different exfoliation pathways namely shearing, pulling and peeling pathways. In a recent study, we have shown that for solvent intercalated h-BN nano-sheets, parallel exfoliation through shearing is preferred over the perpendicular or pulling pathway[19]. Through steered molecular dynamics simulations, Abedini *et al.* suggested that for initially stacked bismuth telluride nano-sheets in ionic liquid, peeling is the most favorable pathway[41]. Keeping the above facts in mind, we calculated the PMF's corresponding to the peeling exfoliation of the materials from a stacked state. Conceptually, re-aggregation is just the opposite process of exfoliation and here the PMF's are calculated as the minimum cumulative reversible work. Therefore, the exfoliation PMF curves also represent lower bounds to the free energies for re-aggregation, but with opposite sign. We calculated the PMF's starting with d_z corresponding to the stacking distance of the respective nano-sheets and distance was increased until the PMF curves reached a platue region and the sheets are completely non-interacting (Fig. 7). It is seen that, for $d_z < 1.8$ nm, the nano-sheets are not completely separated from each other and they always try to maintain a maximum contact area corresponding to a given separation, both in vacuum as well as in solvents (Fig. 7). In fact, we did not observe a situation where the sheets are detached by a single layer or multiple layers of solvent molecules until complete exfoliation and this behavior was similar for all the materials. Fig. 8(a-g) shows the PMF curves scaled to the surface area, corresponding to the exfoliation of all the 2D materials from their respective bilay-

ers in vacuum and in the two solvents as well as the solvent induced lowering of the exfoliation free energies (ΔPMF). For each case, both in water and vacuum, the stacked state is the global minima and a solvent separated minimum do not appear in any of the curves. The vacuum PMF profiles always run below the solvent PMF curves indicating some destabilization of the stacked state encouraged by the solvents, irrespective of their nature. The tendency of exfoliation is given by the trend in ΔPMF, higher magnitude of the quantity indicating preferential inclination towards exfoliation. In both solvents the trend becomes: $MoS_2 \approx$ pseudo $MoS_2 >$ black Pn $\approx$ blue Pn $>$ h-BN $\approx$ pseudo h-BN $>$ graphene, which is nearly in line with the trends in solvation free energies. In addition, for all nano-sheets, exfoliation is preferred in DMSO compared to water, as indicated by higher ΔPMF's in the former solvent. Therefore, the solvent induced lowering of the exfoliation potential well is certainly dictated by the solvophilicity of the 2D materials. During LPE, while a single layer is gradually exfoliated from the bulk, solvent molecules fill the space created between the exfoliating and the penultimate layer, which is otherwise inaccessible. Under
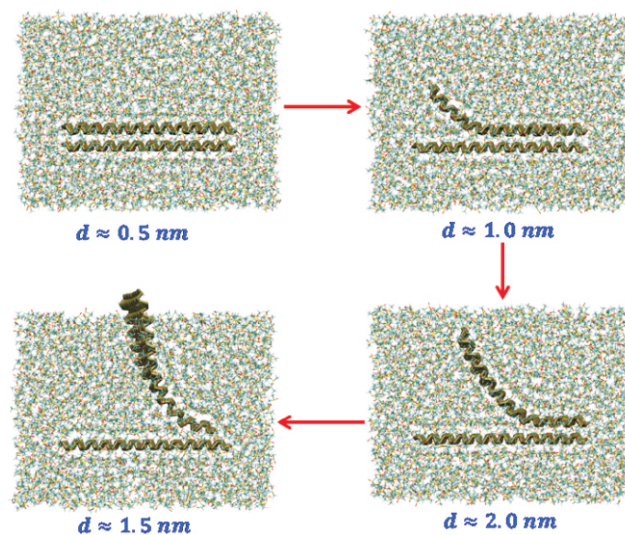

Fig. 7. Snapshots representing the successive conformations obtained during the peeling of a black phosphorene monolayer from a harmonically constrained layer considered to be the penultimate layer of the bulk phase, in presence of DMSO solvent. As peeling progresses, the interlayer gap is filled by the solvent molecules, which help to stabilize the exfoliating and penultimate layer, thereby favoring exfoliation.
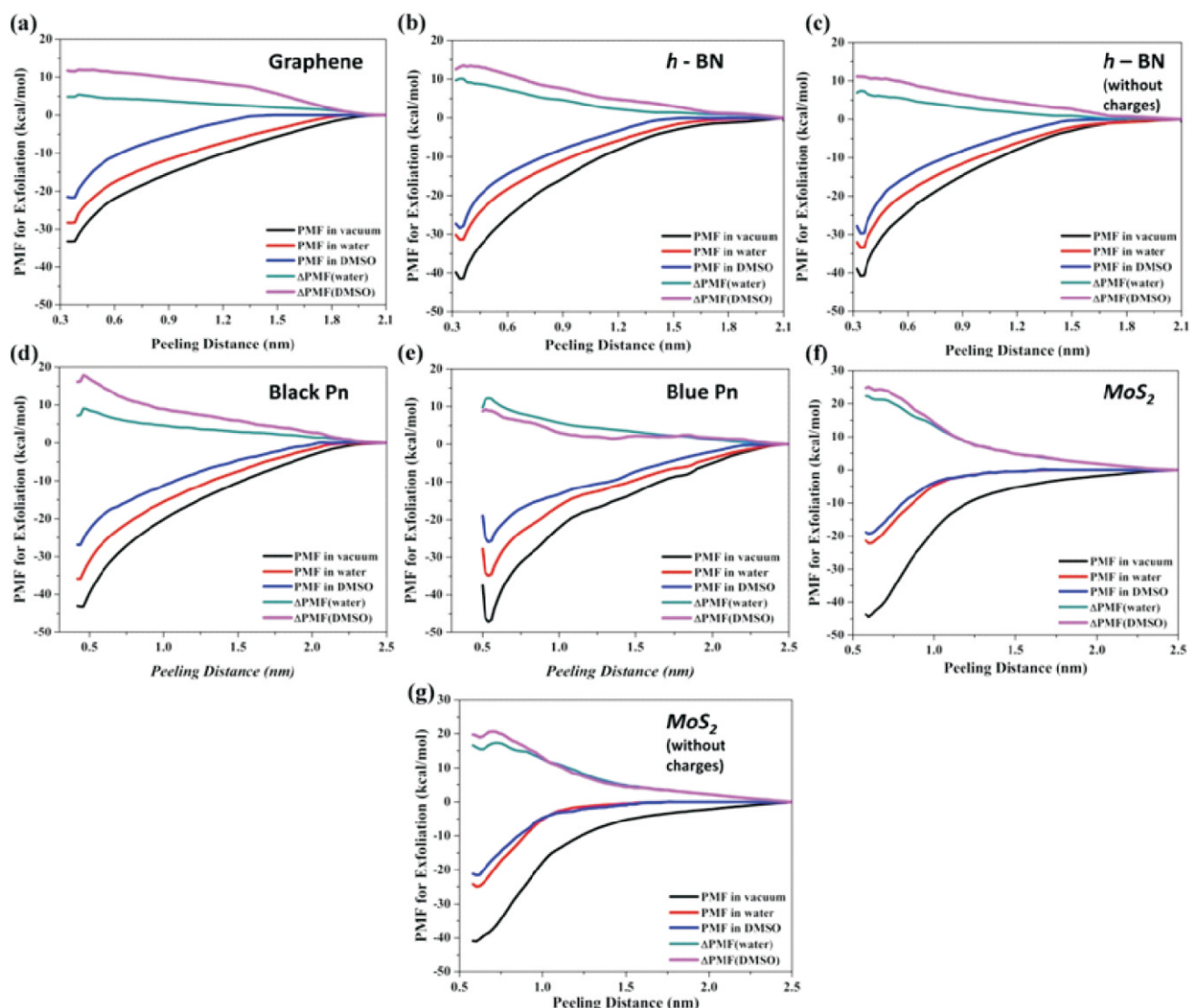
Fig. 8. PMF per unit area for the exfoliation of a nanosheet from a stacked bilayer in vacuum and in presence of solvents water as well as DMSO and ΔPMF, the decrease in free energy penalty for exfoliation in solvents compared to that in vacuum for the 2D materials: (a) graphene, (b) h-BN, (c) h-BN without partial charges (pseudo h-BN), (d) black Pn, (e) blue Pn, (f) MoS_2 and (g) MoS_2 without partial charges (pseudo MoS_2).

such circumstances, not only the interlayer interactions, but the extent of stabilization of the atomically thin exfoliated layer and a newly exposed surface of the bulk material by solvent molecules also govern the ultimate outcome of the sonication experiment.

Conclusions

In summary, we have explored the exfoliation behavior of five 2D materials with different polarities along with diverse extents of dispersion interactions, in polar solvents

namely water and DMSO. Our simulations suggest that, after sonication, the intercalated bulky DMSO molecules interact strongly with the nano-sheets above and below through strong van der Waals interactions, in addition to electrostatic interactions for polar materials, thereby reducing the interlayer interactions, which in turn, reduces the barrier for exfoliation while preventing the collapse of the bilayers. These intercalated solvents behave significantly different from bulk and greatly influence exfoliation as well as re-aggregation. Despite of the polarity, intercalated small water molecules can-

not significantly influence the interlayer interactions of the predominantly hydrophobic 2D materials and therefore, the nano-sheets collapse back into the bilayer state. In water, solvation for most of the 2D crystals is forbidden enthalpically but is driven by a largely favorable entropy change, rendering the total free energy change negative. Solvation in DMSO is exactly opposite it nature, being enthalpically favored but entropically forbidden. Calculation of the work done accompanying exfoliation of the 2D materials show that the effect of partial charge during exfoliation is indeed small and dispersion interaction leads the event. The ease of exfoliation follows similar trend to that of the solvation free energies. Therefore, we can firmly conclude that, a solvent can better exfoliate a 2D material which has higher interfacial stabilization in that solvent and the same quality of the material help to stabilize the dispersed state after successful sonication assisted exfoliation.

Acknowledgement

References

1. J. C. Meyer, A. K. Geim, M. I. Katsnelson, K. S. Novoselov, T. J. Booth and S. Roth, *Nature*, 2007, **446**, 60.

2. K. S. Novoselov, A. K. Geim, S. V. Morozov, D. Jiang, Y. Zhang, S. V. Dubonos, I. V. Grigorieva and A. A. Firsov, *Science*, 2004, **306**, 666.

3. J. S. Bunch, A. M. van der Zande, S. S. Verbridge, I. W. Frank, D. M. Tanenbaum, J. M. Parpia, H. G. Craighead and P. L. McEuen, *Science*, 2007, **315**, 490.

4. K. S. Novoselov, D. Jiang, F. Schedin, T. J. Booth, V. V. Khotkevich, S. V. Morozov and A. K. Geim, *Proc. Natl. Acad. Sci. USA*, 2005, **102**, 10451.

5. C. Huo, Z. Yan, X. Song and H. Zeng, *Science Bullet.*, 2015, **60**, 1994.

6. V. Nicolosi, M. Chhowalla, M. G. Kanatzidis, M. S. Strano and J. N. Coleman, *Science*, 2013, **340**, 1226419.

7. J. N. Coleman, M. Lotya, A. O'Neill, S. D. Bergin, P. J. King, U. Khan, K. Young, A. Gaucher, S. De, R. J. Smith, I. V. Shvets, S. K. Arora, G. Stanton, H.-Y. Kim, K. Lee, G. T. Kim, G. S. Duesberg, T. Hallam, J. J. Boland, J. J. Wang, J. F. Donegan, J. C. Grunlan, G. Moriarty, A. Shmeliov, R. J. Nicholls, J. M. Perkins, E. M. Grieveson, K. Theuwissen, D. W. McComb, P. D. Nellist and V. Nicolosi, *Science*, 2011, **331**, 568.

8. K.-G. Zhou, N.-N. Mao, H.-X. Wang, Y. Peng and H.-L. Zhang, *Angew. Chem. Int. Ed.*, 2011, **50**, 10839.

9. S. Ravula, S. N. Baker, G. Kamath and G. A. Baker, *Nanoscale*, 2015, **7**, 4338.

10. Y. Hernandez, M. Lotya, D. Rickard, S. D. Bergin and J. N. Coleman, *Langmuir*, 2010, **26**, 3208.

11. J. N. Coleman, *Adv. Func. Mater.*, 2009, **19**, 3680.

12. J. Shen, J. Wu, M. Wang, P. Dong, J. Xu, X. Li, X. Zhang, J. Yuan, X. Wang, M. Ye, R. Vajtai, J. Lou and P. M. Ajayan, *Small*, 2016, **12**, 2741.

13. G. Kamath and G. A. Baker, *RSC Advances*, 2013, **3**, 8197.

14. O.-S. Lee and M. A. Carignano, *J. Phys. Chem. C*, 2015, **119**, 19415.

15. V. Sresht, A. Govind Rajan, E. Bordes, M. S. Strano, A. A. H. Pádua and D. Blankschtein, *J. Phys. Chem. C*, 2017, **121**, 9022.

16. V. Sresht, A. A. H. Pádua and D. Blankschtein, *ACS Nano*, 2015, **9**, 8255.

17. C.-J. Shih, S. Lin, M. S. Strano and D. Blankschtein, *J. Am. Chem. Soc.*, 2010, **132**, 14638.

18. A. K. Manna and S. K. Pati, *J. Mat. Chem. B*, 2013, **1**, 91.

19. T. K. Mukhopadhyay and A. Datta, *J. Phys. Chem. C*, 2017, **121**, 811.

20. G. J. Martyna, D. J. Tobias and M. L. Klein, *J. Chem. Phys.*, 1994, **101**, 4177.

21. S. E. Feller, Y. Zhang, R. W. Pastor and B. R. Brooks, *J. Chem. Phys.*, 1995, **103**, 4613.

22. T. Darden, D. York and L. Pedersen, *J. Chem. Phys.*, 1993, **98**, 10089.

23. H. C. Andersen, *J. Comput. Phys.*, 1983, **52**, 24.

24. W. Humphrey, A. Dalke and K. Schulten, *J. Mol. Graph.*, 1996, **14**, 33.

25. L. Kalé, R. Skeel, M. Bhandarkar, R. Brunner, A. Gursoy, N. Krawetz, J. Phillips, A. Shinozaki, K. Varadarajan and K. Schulten, *J. Comput. Phys.*, 1999, **151**, 283.

26. L. Martínez, R. Andrade, E. G. Birgin and J. M. Martínez, *J. Comput. Chem.*, 2009, **30**, 2157.

27. W. L. Jorgensen, J. Chandrasekhar, J. D. Madura, R. W. Impey and M. L. Klein, *J. Chem. Phys.*, 1983, **79**, 926.

28. K. Vanommeslaeghe, E. Hatcher, C. Acharya, S. Kundu, S. Zhong, J. Shim, E. Darian, O. Guvench, P. Lopes and I. Vorobyov, *J. Comput. Chem.*, 2010, **31**, 671.

29. T. K. Mukhopadhyay and A. Datta, *J. Phys. Chem. C*, 2017, **121**, 10210.

30. T. K. Mukhopadhyay and A. Datta, *J. Phys. Chem. C*, 2018, **122**, 28918.

31. E. Darve, D. Rodríguez-Gómez and A. Pohorille, *J. Chem. Phys.*, 2008, **128**, 144120.

32. M. K. Gilson, J. A. Given, B. L. Bush and J. A. McCammon, *Biophys. J.*, 1997, **72**, 1047.

33. T. C. Beutler, A. E. Mark, R. C. van Schaik, P. R. Gerber and W. F. van Gunsteren, *Chem. Phys. Lett.*, 1994, **222**, 529.

34. M. Zacharias, T. P. Straatsma and J. A. McCammon, *J. Chem. Phys.*, 1994, **100**, 9025.

35. P. Liu, F. Dehez, W. Cai and C. Chipot, *J. Chem. Theory Comput.*, 2012, **8**, 2606.

36. G. X. Nie, J. Y. Huang and J. P. Huang, *J. Phys. Chem. B*, 2016, **120**, 9011.

37. C. Chowdhury and A. Datta, *J. Phys. Chem. Lett.*, 2017, **8**, 2909.

38. C. Chowdhury, S. Jahiruddin and A. Datta, *J. Phys. Chem. Lett.*, 2016, **7**, 1288.

39. V. V. Chaban, E. E. Fileti and O. V. Prezhdo, *J. Phys. Chem. C*, 2017, **121**, 911.

40. V. V. Chaban, E. E. Fileti and O. V. Prezhdo, *ACS Nano*, 2017, **11**, 6459.

41. A. Abedini, T. Ludwig, Z. Zhang and C. H. Turner, *Langmuir*, 2016, **32**, 9982.